Composition, stability, and structure of a new member of the aenigmatite group, $Na_2Mg_{4+x}Fe^{3+}_{2-2x}Si_{6+x}O_{20}$, synthesized at 13–14 GPa

TIBOR GASPARIK,[1,]* JOHN B. PARISE,[1] RICHARD J. REEDER,[1]
VICTOR G. YOUNG,[2] AND WENDY S. WILFORD[3]

[1]Center for High Pressure Research and Department of Geosciences, State University of New York at Stony Brook, Stony Brook, New York 11794, U.S.A.
[2]Department of Chemistry, University of Minnesota, Minneapolis, Minnesota 55455, U.S.A.
[3]Department of Chemistry, Whitman College, Walla Walla, Washington 99362, U.S.A.

ABSTRACT

A new phase isostructural with the minerals of the aenigmatite group $Na_2Mg_{4+x}Fe^{3+}_{2-2x}Si_{6+x}O_{20}$ with $x = 0.25 - 0.5$ was synthesized at 13–14 GPa with a split-sphere anvil apparatus (USSA-2000). The structure (for $x = 0.4$) was determined from twinned-crystal X-ray diffraction data. The unit cell is triclinic, $P\bar{1}$, $a = 10.328(1)$, $b = 10.724(1)$, $c = 8.805(1)$ Å, $\alpha = 105.15(1)$, $\beta = 96.85(1)$, $\gamma = 125.47(1)°$, $V = 719.67(3)$ Å^3, $Z = 2$, calculated density = 3.335 g/cm^3. The twin law, independently determined from electron diffraction and transmission electron microscopy and by inspection of the X-ray data collected with an area detector, relates the twin components by a 180° rotation about [110]*. Due to the coupled substitution, $2Fe^{3+} = MgSi$, which introduces octahedral Si, the stability of the phases with the aenigmatite structure apparently expands with increasing pressure. Hence, these phases could play a major role in the transition zone (410–660 km), where the more common minerals they are replacing, olivine and clinopyroxene, reach the limit of their stability. The new evidence for the stability of aenigmatite-like minerals in the deep mantle could have important implications for the origin of the parental magmas producing aenigmatite-bearing and other agpaitic rocks.

INTRODUCTION

Recent advances in seismic tomography provide strong evidence that some or most of the subducted oceanic lithosphere resides in the Earth's transition zone (e.g., van der Hilst et al. 1991; Fukao et al. 1992). Hence, the complete understanding of the transition-zone mineralogy and chemistry must include information on the stability, crystal chemistry, and structure of the phases present at relevant temperatures and pressures as well as sodium-rich compositions typical for the basaltic portion of the oceanic lithosphere. Previous studies in chemically simpler Na-bearing systems (e.g., Gasparik 1989, 1992, 1996; Litvin and Gasparik 1993; Gasparik et al. 1995) are extended here to Fe-bearing compositions that more closely approach the chemical complexity of the Earth's mantle. The primary motivation for this study was to test the prediction of Gasparik and Litvin (1997) that jadeitic clinopyroxene would react with forsterite at a pressure between 13 and 13.5 GPa producing clinoenstatite, garnet, and $Na_2Mg_2Si_2O_7$ (NMS) (Fig. 1). This reaction should cause a major decrease in the temperatures of the anhydrous mantle solidus in the transition zone due to the relatively low melting temperatures of NMS with respect to other mantle phases. In the course of this experimental

investigation, a new Na- and Fe-bearing phase was discovered (Gasparik 1997a), and here we report its structure, chemistry, and stability.

SYNTHESIS TECHNIQUES

Experiments were carried out with a split-sphere anvil apparatus using 10 mm sample assemblies (Gasparik 1989). Lanthanum chromite sleeves were used as the resistance heaters and the samples were enclosed in rhenium capsules. Temperature was measured by a W3%Re vs. W25%Re thermocouple introduced axially and maintained constant during the experiments by a Eurotherm controller. The details of the temperature and pressure calibrations and experimental procedures were given by Gasparik (1989).

Starting materials were mechanical mixtures of high-purity oxides and compounds, including MgO, amorphous SiO_2, Fe metal and synthetic nepheline ($NaAlSiO_4$), fayalite (Fe_2SiO_4), and sodium disilicate ($Na_2Si_2O_5$). The compositions are given in Table 1. The starting materials already loaded in the sample assemblies were dried overnight before the experiments at 100 °C.

After the experiments, the samples still inside the capsules were mounted in epoxy for microprobe analysis. A polished mount contained a lengthwise section of a sample, allowing analysis along the full 200 °C gradient.

FIGURE 1. Subsolidus phase relations in the system NaAl-SiO$_4$-Mg$_2$SiO$_4$-SiO$_2$ at 13 GPa (molar proportions) with the reaction between clinopyroxene and forsterite, producing clinoenstatite, garnet and NMS, indicated by the dashed tie-lines between the reactants and products. Coexisting garnet and NMS are represented by a piercing point where the tie-line between them intersects the ternary plane. Examples of possible mantle compositions include pyrolite (Anderson 1989), cosmic abundancies (Anders and Grevesse 1989), and shell (Gasparik 1997b). Also shown is the composition of the starting material used in experiments 2807 and 2814 (Table 1). Symbols: CEn = clinoenstatite, Cpx = clinopyroxene, En = enstatite, Fo = forsterite, Ga = garnet, Jd = jadeite, Ne = nepheline, NMS = Na$_2$Mg$_2$Si$_2$O$_7$, N2MS = Na$_2$MgSiO$_4$, Py = pyrope. Modified after Gasparik and Litvin (1997).

Wavelength-dispersive chemical analyses were obtained for Na, Fe, Mg, Si, and in some samples for O by a Cameca electron microprobe using 15 kV accelerating potential, beam current of 10 nA, 10 s counting times to minimize the loss of Na and, as standards, natural enstatite for Mg, Si and O, grossular for Al, albite for Na, and fayalite for Fe. The samples were usually well crystallized with the crystal size in the range from 10 to 100 μm, minimizing the possibility of electron beam overlap. The results from microprobe analysis are in Table 1.

SYNTHESIS RESULTS

The first two experiments of Table 1 were carried out at 13 and 13.5 GPa at 1700 °C, using a bulk composition in the system enstatite-forsterite-jadeite (Fig. 1). The results confirmed the prediction of Gasparik and Litvin (1997) that clinopyroxene and forsterite would react between 13 and 13.5 GPa, producing clinoenstatite, garnet, and NMS. Based on the observed compositions of phases in the experimental assemblages, the reaction between 13 and 13.5 GPa can be approximated as follows:

$$16Mg_2SiO_4 + 20Na_{0.5}Mg_{1.1}Al_{0.3}Si_{2.1}O_6$$

$$= 16Mg_2Si_2O_6 + 5Na_{0.4}Mg_{2.8}Al_{1.2}Si_{3.6}O_{12}$$

$$+ 4Na_2Mg_2Si_2O_7. \tag{1}$$

(i.e., forsterite + jadeitic clinopyroxene = clinoenstatite + garnet + NMS).

To test if this reaction would occur in the chemically more complex mantle, additional experiments were carried out with Fe-bearing compositions. The first experiments used starting materials where all Fe was introduced in fayalite. Microprobe analyses of the products from these experiments revealed substantial contents of Fe^{3+}: The cation sums in those phases, which showed excellent stoichiometry in Fe-free experiments, such as pyroxene or garnet (Table 1, runs 2807, 2814), were in significant excess of stoichiometric amounts when all Fe was assumed to be divalent. Amounts of Fe^{3+} were substantially reduced if some of the Fe were introduced in the starting materials as Fe^0 (runs 2825, 2836, 2865). However, the Fe^{3+} contents of pyroxene and garnet were found consistently low or negligible only in those experiments where all Fe was introduced as metal. The probable explanation is that O was continuously introduced into the sample during the experiments, perhaps from the LaCrO$_3$ heater, and the maximum amount of Fe^0 in the sample was essential to buffer the low oxygen fugacity for the whole duration of an experiment.

In the experiments with Fe-bearing compositions, NMS was replaced with a new phase whose composition was originally reported as Na$_{0.7}$Mg$_{1.8}$Fe$^{3+}_{0.3}$Si$_{2.2}$O$_7$ (Gasparik 1997a). This phase was found to be isostructural with aenigmatite, Na$_2$Fe$^{2+}_5$TiSi$_6$O$_{20}$ (Kelsey and McKie 1964). The new phase (Aen) is a solid solution and its compositional variation can be expressed as Na$_2$(Mg, Fe^{2+})$_{4+x}$(Fe^{3+}, Al)$_{2-2x}$Si$_{6+x}$O$_{20}$, where x was observed to vary between 0.25 and 0.5 (Fig. 2). The analyses of Aen (Table 1) were calculated assuming that all Fe was trivalent, but the cation sums for 20 O atoms were in most analyses still in excess of 14. Hence, the amount of Fe^{2+} is likely to be low or negligible. Among the minerals of the aenigmatite group, the closest in composition to one of the theoretical end-members of the new phase, Na$_2$Mg$_4$Fe$^{3+}_2$Si$_6$O$_{20}$, are krinovite, Na$_2$Mg$_4$Cr$_2$Si$_6$O$_{20}$ (Merlino 1972; Bonaccorsi et al. 1989) and wilkinsonite, Na$_2$Fe$^{2+}_4$Fe$^{3+}_2$Si$_6$O$_{20}$ (Ernst 1962; Duggan 1990). However, the observed compositions are stabilized by the coupled substitution 2Fe^{3+} = MgSi, which resembles the substitution in majorite garnet, 2Al = MgSi. This type of substitution requires high pressures, because it introduces octahedral Si. An Fe-free phase marginally resembling the stoichiometry of aenigmatite was also observed at 13 GPa, 1700 °C (run 2814). If this phase also turns out to have the aenigmatite structure, significant vacancy content would be required to satisfy the structural constraints. This phase would also be the closest in composition to the other theoretical end-member, Na$_2$Mg$_5$Si$_7$O$_{20}$, where the substitution of MgSi for 2Fe^{3+} is complete.

TABLE 1. Experimental conditions and average compositions of phases

Run	Mix*	t† (h)	P (GPa)	T (°C)	Phase‡	No.§	Cations					Sum	Ox.‖
							Na	Fe	Mg	Al	Si		
2807	A	5	13.5	1700	Ga	8	0.413	0	2.843	1.128	3.629	8.013	12
					CEn	7	0.043	0	1.915	0.026	2.013	3.997	6
					Fo	6	0.008	0	1.975	0.009	1.003	2.995	4
					NMS	10	1.782	0	1.903	0.081	2.042	5.808	7
2814	A	5	13.0	1700	Ga	15	0.383	0	2.858	1.117	3.638	7.996	12
					Cpx	15	0.486	0	1.115	0.331	2.073	4.005	6
					Fo	6	0.008	0	1.983	0.006	1.002	2.999	4
					Aen	13	2.120	0	5.380	0.305	6.551	14.356	20
2825	B	5	13.5	1700	Ga	10	0.261	0.415	2.587	1.443	3.351	8.057	12
					CEn	5	0.052	0.170	1.809	0.022	1.981	4.034	6
					Cpx	4	0.588	0.238	0.850	0.302	2.082	4.060	6
					Ol	6	0.020	0.199	1.793	0.009	0.992	3.013	4
					Aen	14	1.983	0.725	4.972	0.285	6.260	14.225	20
2836	B	4	13.0	1700	Ga	8	0.272	0.396	2.598	1.206	3.530	8.002	12
					CEn	2	0.045	0.155	1.789	0.052	1.977	4.018	6
					Cpx	12	0.357	0.215	1.146	0.251	2.041	4.010	6
					Ol	3	0.023	0.184	1.796	0.010	0.997	3.010	4
2865	B	2	13.5	1600	Ga	6	0.311	0.468	2.477	1.276	3.493	8.025	12
					CEn	6	0.056	0.176	1.769	0.032	1.989	4.022	6
					Cpx	5	0.644	0.246	0.753	0.326	2.094	4.063	6
					Ol	3	0.039	0.346	1.632	0.017	0.988	3.022	4
					Aen	6	1.956	0.854	4.700	0.281	6.309	14.100	20
2885	C	4	13.5	1650	L	4	1.762	0.435	0.935	0.011	1.866	5.009	6
					CEn	9	0.052	0.237	1.765	0.003	1.984	4.041	6
					NMS	7	1.871	0.501	1.538	0.005	2.009	5.924	7
					Aen	11	2.010	1.411	4.243	0.015	6.307	13.986	20
2892	C	4	13.5	1550	CEn	6	0.035	0.231	1.769	0.001	1.990	4.026	6
					Sp	2	0.010	0.974	1.058	0.001	0.981	3.024	4
					NMS	8	1.855	0.525	1.543	0.001	2.002	5.926	7
					Aen	12	1.951	1.211	4.400	0.003	6.402	13.967	20
2896	C	4	14.0	1550	L	2	1.830	0.335	1.354	0.004	1.695	5.218	6
					CEn	1	0.036	0.222	1.792	0.002	1.983	4.035	6
					CEn	2	0.033	0.208	1.724	0	1.902	3.867	6‖
					NMS	2	1.826	0.422	1.627	0.003	2.016	5.894	7
					NMS	4	2.209	0.385	1.525	0	1.916	6.035	7‖
					Aen	6	1.977	1.108	4.595	0.004	6.374	14.058	20
					Aen	6	2.129	1.066	4.429	0	6.205	13.829	20‖
2902	C	4	13.0	1450	CEn	5	0.055	0.246	1.632	0	1.902	3.835	6‖
					Cpx	4	0.966	0.161	0.390	0	2.324	3.841	6‖
					Sp	6	0.030	1.175	0.834	0	0.915	2.954	4‖
					NMS	8	1.724	0.588	1.385	0	1.909	5.606	7‖
					Aen	15	2.073	0.867	4.532	0	6.236	13.708	20‖

*Bulk compositions (in moles): A = 1 $NaAlSiO_4$, 5 MgO, 4 SiO_2; B = 4 $NaAlSiO_4$, 1 Fe_2SiO_4, 1 Fe°, 17.2 MgO, 14.6 SiO_2; C = 1 $Na_2Si_2O_5$, 1 Fe°, 5 MgO, 4 SiO_2.
† Duration of experiments in hours.
‡ Symbols: Aen = new phase isostructural with aenigmatite, CEn = clinoenstatite, Cpx = jadeitic/acmitic clinopyroxene, Fo = forsterite, Ga = garnet, L = liquid, NMS = $Na_2(Mg, Fe)_2Si_2O_7$, Ol = olivine, Sp = $(Mg, Fe)_2SiO_4$ spinel.
§ The total number of analyses accepted from the given experiment for each phase.
‖ Oxygen content analyzed by electron microprobe. The remaining values are calculated from stoichiometry assuming all Fe as Fe^{3+} in Aen and Fe^{2+} in other phases.

In Fe-bearing compositions, Aen appears between 13 and 13.5 GPa, thus mimicking the appearance of NMS by the reaction of olivine with clinopyroxene in Fe-free compositions. Using the observed compositions of phases in the experimental assemblages (runs 2825, 2836), it is possible to write an analogous reaction producing Aen:

$$4(Mg, Fe^{2+})_2SiO_4$$

$$+ 11Na_{0.4}(Mg, Fe^{2+})_{1.2}Fe^{3+}_{0.14}Al_{0.26}Si_2O_6$$

$$= 3(Mg, Fe^{2+})_2Si_2O_6$$

$$+ 2Na_{0.2}(Mg, Fe^{2+})_{3.1}Al_{1.2}Si_{3.5}O_{12}$$

$$+ 2Na_2(Mg, Fe^{2+})_{4.5}Fe^{3+}_{0.77}Al_{0.23}Si_{6.5}O_{20} \quad (2)$$
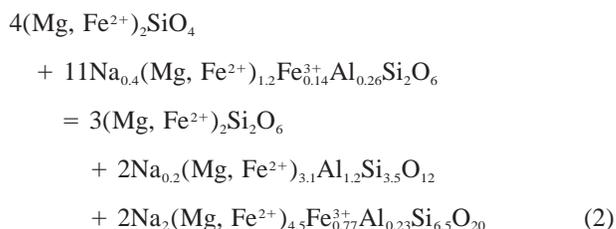
(i.e., olivine + jadeitic clinopyroxene = clinoenstatite + garnet + Aen).

Because the alumina content of Aen was limited, additional experiments were carried out to find out if the Al-free Aen was stable and, possibly, to synthesize single crystals suitable for structure determination. Based on the prior experience, all Fe was introduced as metal and the bulk composition was that originally expected of the unknown phase.

The results from the first three experiments (runs 2885, 2892, 2896) were similar. The samples consisted of three layers: pure clinoenstatite in the hot spot, a mix of colorless clinoenstatite and light-blue NMS in the center, and dark-blue Aen with traces of $(Mg, Fe)_2SiO_4$ spinel in the
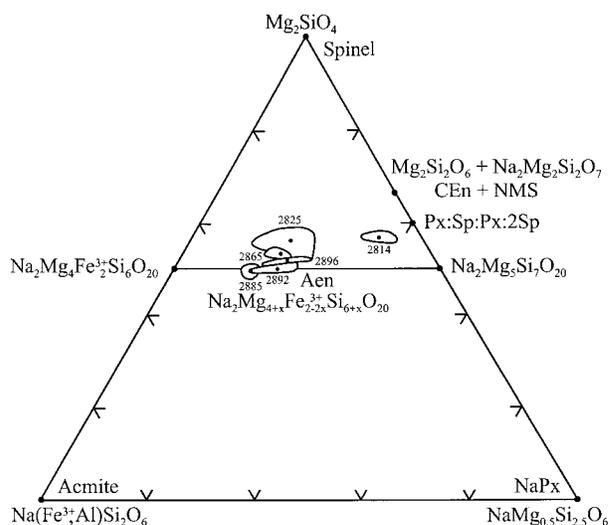
FIGURE 2. Relationships of phases in the system $Na(Fe^{3+},Al)Si_2O_6$-$NaMg_{0.5}Si_{2.5}O_6$-Mg_2SiO_4, including observed variations in the compositions of Aen (envelopes), with averages (dots) and run numbers from Table 1. The compositions of Aen were plotted by calculating the components from the total of Mg + Fe^{3+} + Al + Si = 3: X_{Acmite} = Fe + Al, X_{NaPx} = (4Si − 2Mg − 8Fe − 8Al)/9, X_{Spinel} = (5Mg − Si + 2Fe + 2Al)/9. Also shown for reference is the composition of a hypothetical polysome consisting of "pyroxene" (Px) and "spinel" (Sp) slabs, with 50% of the Sp slabs doubled (Px:Sp:Px:2Sp).

cold end. Quenched liquid could also be present in the hot spot. Apparently, the layering formed in response to the temperature gradient in the sample, producing chemical gradients, including a gradient in the oxygen fugacity (Lesher and Walker 1988; Gasparik and Drake 1995). Using the observed compositions, it is possible to write a redox reaction between the assemblage of clinoenstatite and NMS in the center of the sample, stable at the relatively lower oxygen fugacity, and Aen with spinel in the cold end, representing the product stable at a higher oxygen fugacity:

$$11(Mg, Fe^{2+})_2Si_2O_6 + 4Na_2(Mg, Fe^{2+})_2Si_2O_7 + O_2$$

$$= 4(Mg, Fe^{2+})_2SiO_4 + 4Na_2Mg_{4.5}Fe^{3+}Si_{6.5}O_{20}.$$

$$(3)$$
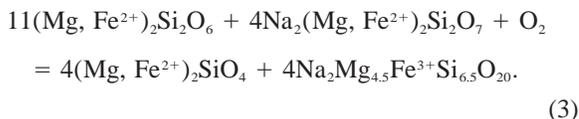
(i.e., clinoenstatite + NMS + oxygen = spinel + Aen).

The experiment at 13 GPa, 1450 °C, (run 2902) showed substantially reduced chemical gradients due to the lower experimental temperature and had clinopyroxene rich in NaPx ($NaMg_{0.5}Si_{2.5}O_6$). This experimental product and the product from 2896 were also analyzed by the electron microprobe for oxygen. The results for Aen suggest deviations from stoichiometry, which could be explained by the presence of O vacancies. This is supported by the observed excess of Mg and deficiency in Si with respect to the ideal formula in most analyses of Aen, thus maintaining the charge balance in the presence of oxygen vacancies. Surprisingly, the pyroxene analyses also suggest the possible presence of vacancies. However, the data are limited and more analyses are needed to confirm these results.

STRUCTURE DETERMINATION

Diffraction data were collected from a presumed single crystal (0.13 mm × 0.04 mm × 0.03 mm) of Aen from experiment 2892, attached to a glass fiber and mounted on a Siemens SMART X-ray diffractometer. A randomly oriented region of reciprocal space was surveyed to the extent of 1.5 hemispheres to a resolution of 0.84 Å. Three major swaths of frames were collected with 0.30° steps in Ω. An initial set of cell constants was calculated from reflections harvested from four sets of 30 frames; these were consistent with a C-centered monoclinic cell. However, the discrepancy factors were too large, for example, R_F = 0.12 for $F > 4 \sigma(F)$, and the structure model also contained several partially occupied sites centered in edge and face shared polyhedra. Twinning was suspected in the crystal used for data collection.

Ion-thinned foils of a fresh second sample of Aen from experiment 2896 were examined using a JEOL 200CX TEM operated at 200 keV. Imaging revealed the presence of pervasive lamellae (Fig. 3). A smaller triclinic cell [a = 8.7912(2), b = 9.6399(3), c = 10.3152(3) Å, α = 64.847(1), β = 83.150(2), γ = 65.308(1)°] was found to be consistent with both the TEM results and with the X-ray data (see below), if a 180° rotation twin axis about [110]* was present. Indeed, the lamellae in Figure 3 are parallel to (110) and are observed in all grains examined. The lamellar widths range from several tens to hundreds of nanometers with lamellae-free regions rarely exceeding 2 μm in width. Comparison of SAED from lamellar regions with adjacent lamellae-free areas revealed the appearance of extra spots (Fig. 3c) in alternate rows parallel to [110]*, consistent with a twin either on (110) or by 180° rotation about [110]*. Superposition of some spots also occurred. The pervasive nature of the twin lamellae suggested formation by phase transformation, perhaps during quenching. Foils showed evidence of irradiation damage after a short period of imaging.

The X-ray data were reinvestigated to determine whether the specimen used for the original data collection was twinned. Dirax (Duisenberg 1992) was used to index the two twin components found in the TEM work (Table 2) from 50 randomly chosen reflections. All reflections indexed to one or both twin components. This reduced triclinic unit cell does not transform to any higher crystal system. The separate orientation matrices determined were used to integrate two independent data files with SAINT (Bruker AXS 1994a). The cell constants determined by least-squares from a set of ~3500 reflections for the twin components are as follows: a = 8.8054(7), b = 9.6516(8), c = 10.3284(8) Å, α = 64.822(1), β = 83.146(1), and γ = 65.290(1)° for twin component 1, and a = 8.7912(2), b = 9.6399(3), c = 10.3152(3) Å, α = 64.847(1), β = 83.150(2), and γ = 65.308(1)° for twin component 2. The twin law relating the twin components
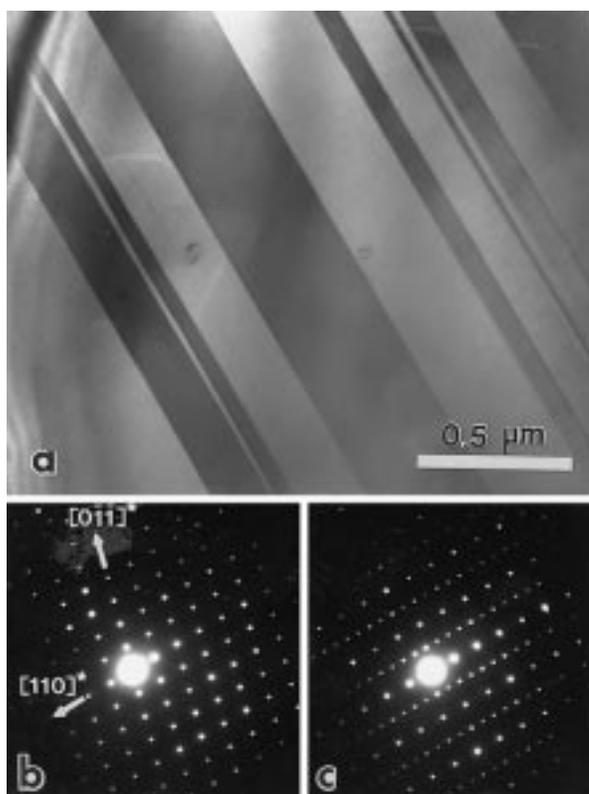
FIGURE 3. Brightfield TEM image showing pervasive twin lamellae parallel to (110) in Aen **a**, and selected-area electron diffraction patterns for a rare twin-free region **b** and the adjacent area containing lamellae **c**. Extra spots appearing in alternate rows parallel to [110]* in **c** are the result of twinning. Indices refer to the reduced triclinic cell (see text), which is related to the previously reported setting for aenigmatite-like minerals by the transformation (by rows): 0,0,1;0,1,-1;-1,0,0.

TABLE 2. Crystal data and details of the structure refinement for Aen

Parameter	Value
Formula	$Na_2[Mg_{4.4}Si_{0.4}Fe_{1.2}]Si_6O_{20}$
Crystal habit, color	Plate, light blue, pleochroic
Crystal size	$0.13 \times 0.05 \times 0.03$ mm
Crystal system, space group	triclinic, $P\bar{1}$
	$a = 10.328(1)$, $b = 10.724(1)$,
	$c = 8.805(1)$ Å, $\alpha = 105.15(1)$,
	$\beta = 96.85(1)$, $\gamma = 125.47(1)°$
Volume	$719.67(3)$ Å³
Formula weight	722.7
Z	2
Calculated density	3.335 Mg/m³
Absorption coefficient	2.23 mm⁻¹
Diffractometer	Siemens SMART Platform CCD
Wavelength	0.71073 Å
Temperature	298(2) K
θ range for data collection	2.19 to 25.08°.
Index ranges	$-12 \leq h \leq 12$, $-12 \leq k \leq 12$, $-10 \leq l \leq 10$
Reflections collected	3653
Independent	2450
Refinement system used	SHELXL (Bruker 1994b)
Solution	Direct Methods
Refinement method	Full-matrix least-squares on F^2
Weighting scheme	$w = [\sigma^2(F_o^2) + (AP)^2 + (BP)]^{-1}$, where $P = (F_o^2 + 2F_c^2)/3$, A = 0.0742 and B = 0.0
Absorption correction	SADABS (Blessing 1995)
Rel. Max./min. transmission	1.000 and 0.746
Extinction coefficient	0.0028(10)
Data/restraints/parameters	2450/1/319
Goodness-of-fit on F^2	0.946
Final R indices $[I > 2\sigma(I)]$	$R_1 = 0.0348$, $wR_2 = 0.0962$
R indices (all data)	$R_1 = 0.0440$, $wR_2 = 0.1007$
Largest diff. peak and hole	0.530, −0.580 e.Å³; 0.7 and 0.6 Å from Si2 and Mg7, respectively

is, by rows, $[0,1,-1/2;1,0,-1/2;0,0,-1]$. The twin components are related by a 180° rotation about [110]*; the rotation axis in direct space, [22−1], was found by TWROT (R.A. Sparks, private communication). SAD-ABS (Blessing 1995) was used to correct the data for the effects of X-ray absorption. The space group ($P\bar{1}$) was determined, based on intensity statistics. A successful direct-methods solution (Bruker AXS 1994b) was calculated with data uncorrected for the contribution of the twin component. A complete structural model was obtained from least squares and calculation of Fourier difference maps before final refinement proceeded with corrected data. UNTWIN (Young 1997) was used to produce data corrected for both twin components based on the twin law. These data were produced in the form of SHELXL HKLF 5 data (Bruker AXS 1994b) where reflections with a contribution from the second twin component are refined with the addition of a single scale factor. Data from both twin components were refined in this way; there is no substantial difference in these models. The positional parameters and selected interatomic distances are given

in Tables 3 and 4, respectively. Anisotropic displacement parameters are given in Table 5. Calculated and observed values are in Table 6.[1]

Following the solution of its structure, it became clear that the new phase was isostructural with the minerals of the aenigmatite group (Cannillo et al. 1971; Bonaccorsi et al. 1990), although its identification was delayed by the fact that the unit cell customarily used in the literature for the minerals of the aenigmatite group (e.g., Deer et al. 1978) is not the conventional cell and does not possess the shortest non-coplanar translations. The conventional cell can be related to the customary setting by the trasformation matrix (by rows): 0,0,1;0,1,−1;−1,0,0 and results in the cell: $a = 10.328(1)$, $b = 10.724(1)$, $c = 8.805(1)$ Å, $\alpha = 105.15(1)$, $\beta = 96.85(1)$, $\gamma = 125.47(1)°$.

Because the mineral aenigmatite, $Na_2Fe_5TiSi_6O_{20}$, is reported to have Ti ordered into one of the octahedral M sites (Table 3), attempts were made to investigate the possibilities for site ordering in Aen, although there was little evidence for it in the initial refinement. Based on the general formula $X_2M_6T_6O_{20}$, it was assumed that all anion and

---

[1] For a copy of Table 6, document item AM-98-005, contact the Business Office of the Mineralogical Society of America (see inside front cover of recent issue) for price information. Deposit items may also be available on the American Mineralogist web site at http://www.minsocam.org.

TABLE 3. Atomic coordinates ($\times 10^4$) and equivalent isotropic displacement parameters ($\text{Å}^2 \times 10^3$)

Atom	x	y	z	U_{eq}†
M1*	0	0	5000	13(1)
M2*	0	5000	0	15(1)
M3*	3139(3)	8489(3)	1780(3)	10(1)
M4*	7687(2)	8191(3)	1508(3)	8(1)
M5*	949(4)	9394(3)	559(3)	12(1)
M6*	5959(3)	9422(3)	646(3)	9(1)
M7*	9920(2)	7350(2)	2649(2)	8(1)
Si1	4767(3)	2328(3)	3320(3)	6(1)
Si2	9836(3)	2339(3)	3451(3)	8(1)
Si3	7910(3)	3428(3)	2402(3)	7(1)
Si4	2793(3)	3399(3)	2254(3)	6(1)
Si5	6497(2)	9493(2)	4436(2)	7(1)
Si6	3549(2)	5602(2)	458(2)	6(1)
Na1	2093(4)	6344(4)	3911(4)	14(1)
Na2	6621(4)	6118(4)	3698(4)	14(1)
O1	3555(7)	650(7)	1628(7)	8(1)
O2	8600(7)	659(7)	1743(7)	10(1)
O3	5595(7)	9605(7)	2915(7)	10(1)
O4	255(8)	9357(9)	2693(8)	21(2)
O5	2314(7)	8718(7)	3902(7)	7(1)
O6	7486(7)	8827(7)	3901(7)	9(1)
O7	4926(6)	1955(7)	4984(6)	10(1)
O8	9556(7)	7774(7)	4830(7)	16(1)
O9	8970(7)	3218(7)	3701(7)	13(1)
O10	4029(6)	3363(7)	3533(6)	7(1)
O11	6588(7)	1729(7)	694(7)	9(1)
O12	1538(7)	1675(7)	617(7)	8(1)
O13	5289(7)	7104(7)	353(7)	9(1)
O14	605(7)	7288(7)	654(8)	14(1)
O15	2426(7)	6133(7)	1125(7)	9(1)
O16	7512(8)	6099(8)	1283(8)	16(1)
O17	4034(6)	5015(6)	1889(6)	8(1)
O18	9347(7)	5112(7)	2243(7)	12(1)
O19	1664(6)	3696(7)	3195(7)	9(1)
O20	6738(6)	3666(7)	3372(7)	7(1)

* Site occupancies (x) of M1–M7 are (in order) 0.749(4), 0.702(4), 0.760(4), 0.787(4), 0.831(4), 0.791(4), 0.806(4) for the substitution (Mg, Si)$_x$Fe$_{1-x}$.
† U_{eq} is defined as one third of the trace of the orthogonalized U_{ij} tensor.

TABLE 4. Selected interatomic distances (Å) for Aen

Atom	Distance	Atom	Distance
M1-O6*	2.058(6)	M2-O15	1.995(5)
M1-O6†	2.058(6)	M2-O15#	1.995(5)
M1-O4‡	2.068(7)	M2-O14	2.034(6)
M1-O4§	2.068(7)	M2-O14#	2.034(6)
M1-O8*	2.111(6)	M2-O18**	2.158(6)
M1-O8†	2.111(6)	M2-O18‖	2.158(6)
⟨M1-O⟩	2.079	⟨M2-O⟩	2.062
M3-O3	2.028(6)	M4-O13	1.990(6)
M3-O15	2.058(6)	M4-O16	2.096(7)
M3-O14	2.072(6)	M4-O6	2.113(6)
M3-O1††	2.144(6)	M4-O4‡‡	2.120(7)
M3-O5	2.159(6)	M4-O12**	2.128(6)
M3-O11**	2.199(6)	M4-O2††	2.170(6)
⟨M3-O⟩	2.110	⟨M4-O⟩	2.103
M5-O12#	2.076(6)	M6-O3	2.058(6)
M5-O4	2.092(7)	M6-O13	2.086(6)
M5-O14	2.099(6)	M6-O1**	2.114(6)
M5-O1††	2.114(6)	M6-O11**	2.137(6)
M5-O2**	2.127(7)	M6-O11††	2.149(7)
M5-O12††	2.136(7)	M6-O2††	2.153(6)
⟨M5-O⟩	2.107	⟨M6-O⟩	2.116
M7-O5‡‡	1.943(6)	Na1-O18‖	2.364(6)
M7-O4‡‡	1.961(7)	Na1-O7*	2.365(5)
M7-O14‡‡	1.970(7)	Na1-O5	2.422(6)
M7-O8	1.988(6)	Na1-O15	2.487(6)
M7-O16	2.001(6)	Na1-O19	2.490(6)
M7-O18	2.022(6)	Na1-O9*	2.546(7)
⟨M7-O⟩	1.981	Na1-O20*	2.554(6)
		Na1-O9‖	2.943(6)
Si1-O1	1.601(6)		
Si1-O7	1.631(6)	Na2-O17	2.326(6)
Si1-O10	1.660(5)	Na2-O8	2.333(6)
Si1-O20	1.661(6)	Na2-O16	2.416(7)
⟨Si1-O⟩	1.638	Na2-O6	2.439(6)
Si2-O2	1.610(6)	Na2-O10	2.534(6)
Si2-O9	1.630(6)	Na2-O10*	2.611(6)
Si2-O8§§	1.630(6)	Na2-O20	2.645(7)
Si2-O19‡‡	1.679(6)	Na2-O19*	2.968(6)
⟨Si(2)-O⟩	1.637		
Si3-O18	1.598(6)	Si5-O6	1.600(6)
Si3-O11	1.623(6)	Si5-O3	1.610(6)
Si3-O9	1.637(6)	Si5-O5‖‖	1.643(6)
Si3-O20	1.658(5)	Si5-O7*	1.666(5)
⟨Si3-O⟩	1.629	⟨Si5-O⟩	1.630
Si4-O12	1.599(6)	Si6-O13	1.609(6)
Si4-O17	1.600(6)	Si6-O16**	1.642(6)
Si4-O10	1.623(6)	Si6-O15	1.664(5)
Si4-O19	1.634(5)	Si6-O17	1.693(5)
⟨Si4-O⟩	1.614	⟨Si6-O⟩	1.652

Notes: Symmetry transformations used to generate equivalent atoms: (*) $-x+1,-y+1,-z+1$; (†) $x-1,y-1,z$; (‡) $-x,-y+1,-z+1$; (§) $x,y-1,z$; (‖) $x-1,y,z$; (#) $-x,-y+1,-z$; (**) $-x+1,-y+1,-z$; (††) $x,y+1,z$; (‡‡) $x+1,y,z$; (§§) $-x+2,-y+1,-z+1$; (‖‖) $-x+1,-y+2,-z+1$.

cation sites were fully occupied (by using linear constraints), sites X and T were only occupied by Na and Si, respectively, and no distinction was made between the scattering of Mg and Si occupying the M sites. Initially, the occupancies of M1-M7 (Table 3) were allowed to vary with no constraint on composition, and this resulted in a model with the formula $Na_2[(Mg, Si)_{4.9}Fe_{1.1}]Si_6O_{20}$, which is in agreement with that determined from the microprobe analysis $Na_2[Mg_{4.4}Si_{0.4}Fe_{1.2}]Si_6O_{20}$. Refinements in which Fe^{3+} was constrained to fully occupy one of the M sites (Table 3) resulted in R_F values above 0.12. These models also had unrealistically large and small (negative!) displacement ellipsoids for those M sites occupied by Fe and (Mg, Si), respectively. However, one site (M7, Table 4) is significantly smaller than the others, <M7-O> = 1.98 whereas <M-O> = 2.10, which suggests it might be enriched in either Fe^{3+} and/or Si. The site is considerably larger than would be expected if it were occupied exclusively by Si (Angel et al. 1988; Pacalo and Parise 1992; Gasparik et al. 1995).

DISCUSSION OF THE STRUCTURE

The structure of Aen is composed of two types of layers (Fig. 4), stacked alternately along [011]. One layer (Fig. 4a) consists of slabs of edge-shared octahedra alternating with bands of edge-sharing Na-centered polyhedra. The second layer (Fig. 4b) consists of open-branched vierer single chains (Liebau 1985) of corner-shared SiO_4 tetrahedra linked by isolated (Mg, Si, Fe^{3+})-centered octahedra (M2 and M1 in Fig. 4b). A polyhedral view of the structure is shown in Figure 5.

Polysomatic relationship in materials with the aenigmatite structure, specifically in rhönite, was described by Bonaccorsi et al. (1990). The structure consists of ordered 1:1 intergrowth of spinel- and pyroxene-type structural elements or slabs (Fig. 6) with compositions $M_4Si_2O_8$ and $Na_2M_2Si_4O_{12}$, respectively, where M = (Mg, Si, Fe^{3+}). While the observed composition and the TEM observa-

TABLE 5. Anisotropic displacement parameters ($\mathring{A}^2 \times 10^3$) for Aen

Atom	U_{11}	U_{22}	U_{33}	U_{23}	U_{13}	U_{12}
M1	12(1)	9(1)	15(1)	−1(1)	−3(1)	8(1)
M2	10(1)	13(1)	14(1)	0(1)	4(1)	5(1)
M3	12(1)	11(1)	10(1)	5(1)	5(1)	8(1)
M4	8(1)	8(1)	7(1)	2(1)	2(1)	5(1)
M5	9(1)	15(1)	13(1)	7(1)	6(1)	7(1)
M6	9(1)	11(1)	7(1)	5(1)	5(1)	6(1)
M7	7(1)	7(1)	8(1)	0(1)	0(1)	5(1)
Si1	8(1)	10(1)	4(1)	4(1)	3(1)	6(1)
Si2	9(1)	11(1)	8(1)	6(1)	4(1)	7(1)
Si3	7(1)	11(1)	3(1)	3(1)	3(1)	6(1)
Si4	7(1)	8(1)	4(1)	3(1)	3(1)	5(1)
Si5	8(1)	6(1)	8(1)	4(1)	3(1)	4(1)
Si6	8(1)	5(1)	7(1)	2(1)	2(1)	4(1)
Na1	13(2)	11(1)	14(1)	5(1)	1(1)	6(1)
Na2	11(2)	14(1)	20(2)	10(1)	6(1)	8(1)
O1	7(3)	9(3)	10(3)	7(2)	6(2)	5(2)
O2	7(3)	11(3)	16(3)	7(2)	4(2)	7(2)
O3	6(2)	12(2)	8(2)	4(2)	0(2)	5(2)
O4	24(3)	30(3)	10(3)	3(2)	0(2)	20(3)
O5	10(2)	4(2)	6(3)	1(2)	2(2)	6(2)
O6	10(2)	5(2)	11(3)	4(2)	3(2)	5(2)
O7	7(3)	13(2)	9(2)	5(2)	5(2)	6(2)
O8	11(3)	14(2)	17(3)	9(2)	−2(2)	5(2)
O9	13(3)	14(3)	12(3)	1(2)	4(2)	10(2)
O10	9(2)	9(2)	7(2)	3(2)	5(2)	6(2)
O11	11(3)	5(3)	5(3)	−2(2)	1(2)	4(2)
O12	11(3)	5(3)	6(3)	−2(2)	0(2)	3(2)
O13	13(2)	6(2)	7(2)	1(2)	4(2)	6(2)
O14	6(3)	11(3)	25(3)	4(2)	1(2)	7(2)
O15	8(2)	10(3)	7(2)	0(2)	−1(2)	7(2)
O16	13(3)	7(3)	14(3)	−2(2)	4(2)	3(2)
O17	8(2)	5(2)	9(2)	2(2)	4(2)	3(2)
O18	7(2)	18(3)	11(2)	10(2)	3(2)	7(2)
O19	7(3)	4(2)	13(3)	3(2)	5(2)	2(2)
O20	5(2)	7(2)	5(2)	0(2)	3(2)	2(2)

Note: The anisotropic displacement factor exponent takes the form: $-2\pi^2[h^2a^{*2}U_{11} + \ldots + 2hka^*b^*U_{12}]$.

(a)

(b)

FIGURE 4. Polyhedral representation of the structure of Aen viewed down [111]: dashed lines represent the outline of the unit cell, **a** and **b** show the two types of layers that stack along [011] to form the structure.

tions of the sample of Aen used for the structure determination suggest that it has the ideal stoichiometry of the aenigmatite structure consistent with the 1:1 polysome, other chemically more complex samples of Aen listed in Table 1 show significant solubility of $M_4Si_2O_8$, consistent with polysomes having up to 50% of the spinel slabs doubled (Fig. 2).

The coordination environments about anions and cations in Aen (Table 4, Figs. 4 and 6) are similar to those found in other minerals of the aenigmatite group (Bonaccorsi et al. 1989) with the following qualifiers: (1) In Aen, the distribution of <Na-O> distances in both Na-centered polyhedra is (5+2+1) with five at 2.3–2.5 Å, two at 2.5–2.6 Å and one greater than 2.9 Å. As in the case of aenigmatite, the coordination polyhedron is intermediate between a cube and square antiprism, but there is only one rather than two distinctly longer Na-O distance in each Na-polyhedron (Table 4). (2) In the open-branched single vierer chain (Liebau 1985; Figs. 4 and 6), the distribution of distances (Table 4) generally follows trends expected from valence considerations (Bonaccorsi et al. 1989). The longer distances are associated with O atoms, which bridge two silicon atoms, whereas the shorter distances are associated with terminal O atoms

bonded to only one Si and lower-valent cations (Na⁺, Mg²⁺/Fe³⁺). This distribution in distances for the silicate tetrahedra and the average <Si-O> distances are in particularly good agreement with those reported for the mineral krinovite, $Na_2Mg_4Cr_2Si_6O_{20}$ (Bonaccorsi et al. 1989).

The origin of the twinning, particularly when it formed during the experiments, remains uncertain. It seems unlikely that the twins resulted from plastic deformation associated with depressurization of the cell assembly, because no other deformation microstructure was observed, and the same type of twinning is common in the minerals of the aenigmatite group. It is possible that the pervasive distribution of the twins and the limited range of lamellar widths could be caused by a structural phase transition, as proposed by Kelsey and McKie (1964). If this were the case, then the twins would indicate a symmetry reduction, possibly during quenching. On the basis of the twin operation, a 180° rotation about [110]*, a possible
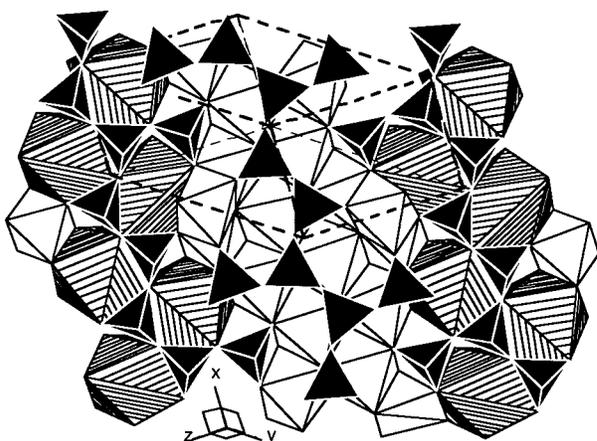
FIGURE 5. Polyhedral representation of the structure of Aen projected down [122]. Only two of the layers from Figure 4 are shown for clarity.

space group symmetry for the high-temperature polymorph is $C2/c$. On the other hand, Cannillo et al. (1971) considered the stability of a monoclinic polymorph unlikely and proposed a primary origin for the twinning by metastable crystallization of twinned aenigmatite at high temperatures.

IMPLICATIONS FOR THE EARTH'S MANTLE

This study produced the first evidence for the stability of phases isostructural with aenigmatite at the pressures and temperatures thought to exist in the Earth's transition zone. Thus, the stability of the known minerals of the aenigmatite group could be much greater than was evident so far. A complete solid solution is possible between the two Na-bearing minerals of the aenigmatite group found to occur on Earth, aenigmatite and wilkinsonite (Duggan 1990), although limited solubility was also observed (Gaeta and Mottana 1991). In this case, the substitution is $2Fe^{3+} = Fe^{2+}Ti$. It is possible that complete solubility exists between these minerals and the new high-pressure phase, although at some pressures and temperatures only intermediate compositions might be stable. In this case, the substitutions would be $Fe^{2+} = Mg$ and $Ti = Si$. It is common to find in other structures that the Fe end-member compositions become stable at lower pressures than the Mg end-members of the same structure, for example, Fe_2SiO_4 vs. Mg_2SiO_4 spinel (Ringwood and Major 1966), or the high-pressure polymorphs of clinoferrosilite vs. clinoenstatite (Pacalo and Gasparik 1990; Woodland and Angel 1997). The substitution of octahedral Si for Ti with increasing pressure is also common, for example, $CaTiO_3$ vs. $CaSiO_3$ perovskite (Ringwood and Major 1971; Kubo et al. 1997; Leinenweber et al. 1997) and $CaTiSiO_5$ vs. $CaSi_2O_5$ titanite (Kanzaki et al. 1991; Knoche et al. 1998). Complete or extensive solid solution often occurs between the low-pressure and high-pressure end-members with these types of substitutions, making it likely that intermediate compositions with the
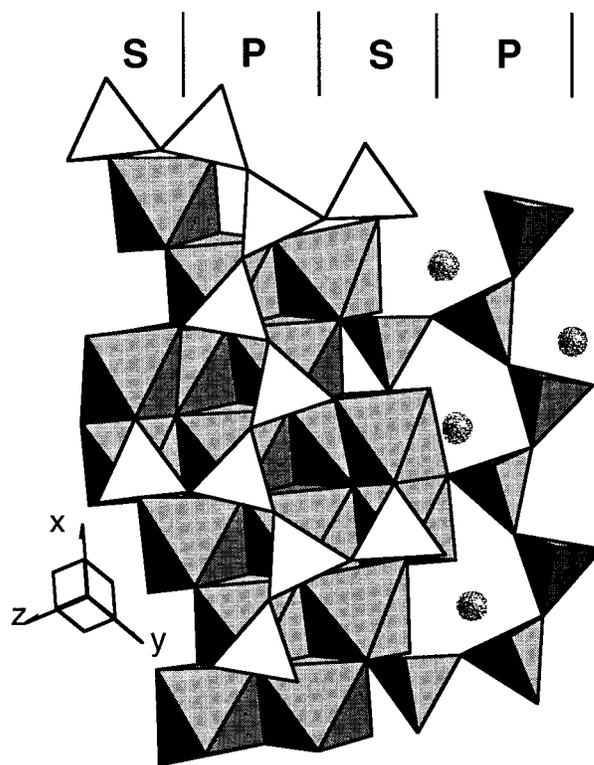
FIGURE 6. Intergrowth of the "pyroxene" (P) and "spinel" (S) slabs, which constitute the aenigmatite structure. The spheres represent Na^+ cations. After Bonaccorsi et al. (1990).

aenigmatite structure are stable in the whole pressure-temperature range of the mantle from one bar to the transition zone. The stability of the aenigmatite-like phases is also likely to increase with increasing pressure due to the substitution of MgSi for $2Fe^{3+}$. This substitution introduces octahedral Si into the structure and thus is similar to the majorite substitution of MgSi for 2Al, which is known to cause substantial expansion in the stability of garnet with pressure (Ringwood 1967; Gasparik 1989). Hence, the phases with the aenigmatite structure could play a much more important role in the deeper mantle than in the Earth's crust.

The observation that Aen replaces NMS in Fe-bearing compositions could have important implications for the origin of the parental magmas producing peralkaline rocks. Gasparik and Litvin (1997) proposed that NMS should be the solidus phase in the deeper mantle, replacing nepheline outside its stability. They reported that Na and Al, which at lower pressures are typically coupled in mantle minerals, such as albite ($NaAlSi_3O_8$), jadeite ($NaAlSi_2O_6$), and nepheline ($NaAlSiO_4$), can decouple at pressures higher than the stability of nepheline with Al preferentially incorporated in garnet and Na in Na-rich and Al-poor phases, such as NMS. It now appears, that in the presence of Fe, the Na-rich and Al-poor phases replacing nepheline at the solidus at higher pressures could include aenigmatite. Since the Na-rich and Al-poor

phases have melting temperatures much lower than other coexisting mantle phases, the first melts are bound to have compositions similar to these Na-rich phases. Thus, some parental magmas producing aenigmatite-bearing and other agpaitic rocks may have originated at greater depths than the nepheline-normative alkali basaltic melts. This could include the magmas responsible for the alkaline volcanism associated with the rifting of thick continental lithosphere (Gasparik and Litvin 1997).

Reaction 2 between olivine and clinopyroxene, producing clinoenstatite, garnet, and Aen, occurs at the pressures corresponding to ~400 km depth and could potentially produce a sharp discontinuity in seismic velocities consistent with the seismic observations of the 410 km discontinuity (Benz and Vidale 1993). To further test the viability of this alternative mechanism, the effects of other elements likely to be present in the mantle on the reaction need to be investigated. While some elements, such as Ca, are likely to stabilize clinopyroxene, other elements, such as Ti, Cr, and Mn, are more likely to stabilize the minerals of the aenigmatite group. Hence, the full evaluation of the potential viability of the proposed mechanism as an explanation for the 410 km discontinuity requires experiments with the compositions reflecting the full potential chemical complexity of the Earth's mantle.

REFERENCES CITED

Anders, E. and Grevesse, N. (1989) Abundances of the elements: meteoritic and solar. Geochimica et Cosmochimica Acta, 53, 197–214.
Anderson, D.L. (1989) Theory of the Earth. Blackwell, Oxford, 366 p.
Angel, R.J., Gasparik, T., Ross, N.L., Finger, L.W., Prewitt, C.T., and Hazen, R.M. (1988) A silica-rich sodium pyroxene phase with six-coordinated silicon. Nature, 335, 156–158.
Benz, H.M. and Vidale, J.E. (1993) Sharpness of upper-mantle discontinuities determined from high-frequency reflections. Nature, 365, 147–150.
Blessing, R. (1995) An empirical correction for absorption anisotropy. Acta Crystallographica (vol. A51), 33–38.
Bonaccorsi, E., Merlino, S., and Pasero, M. (1989) Crystal structure of the meteoritic mineral krinovite, NaMg₂CrSi₃O₁₀. Zeitschrift für Kristallographie, 187, 133–138.
———(1990) Rhönite: structural and microstructural features, crystal chemistry, and polysomatic relationships. European Journal of Mineralogy, 2, 203–218.
Bruker, AXS (1994a) SAINT V4 program for reduction of data collected on Bruker AXS CCD area detector systems. Bruker AXS, Madison, WI.
———(1994b) SHELXL V5 program suite for the solution and refinement of crystal structures. Bruker AXS, Madison, WI.
Cannillo, E., Mazzi, F., Fang, J.H., Robinson, P.D., and Ohya, Y. (1971) The crystal structure of aenigmatite. American Mineralogist, 56, 427–446.
Deer, W.A., Howie, R.A., and Zussman, J. (1978) Rock-forming minerals. Single chain silicates. Wiley, New York, 668 p.
Duggan, M.B. (1990) Wilkinsonite, Na₂Fe₄²⁺Fe₂³⁺Si₆O₂₀, a new member of the aenigmatite group from the Warrumbungle volcano, New South Wales, Australia. American Mineralogist, 75, 694–701.
Duisenberg, A.J.M. (1992) Indexing in single-crystal diffractometry with an obstinate list of reflections. Journal of Applied Crystallography, 25, 92–96.
Ernst, W.G. (1962) Synthesis, stability relations, and occurrence of riebeckite and riebeckite-arfvedsonite solid solutions. Journal of Geology, 70, 689–736.
Fukao, Y., Obayashi, M., Inoue, H., and Nenbai, M. (1992) Subducting slabs stagnant in the mantle transition zone. Journal of Geophysical Research, 97, 4809–4822.
Gaeta, M. and Mottana, A. (1991) Phase relations of aenigmatite minerals in a syenitic ejectum, Wonchi volcano, Ethiopia. Mineralogical Magazine, 55, 529–534.
Gasparik, T. (1989) Transformation of enstatite-diopside-jadeite pyroxenes to garnet. Contributions to Mineralogy and Petrology, 102, 389–405.
———(1992) Enstatite-jadeite join and its role in the Earth's mantle. Contributions to Mineralogy and Petrology, 111, 283–298
———(1996) Diopside-jadeite join at 16–22 GPa. Physics and Chemistry of Minerals, 23, 476–486.
———(1997a) Discovery of Na₀.₇Mg₁.₈Fe₀.₃³⁺Si₂.₂O₇: possible major mineral constituent of the upper mantle. Eos, 78, Spring Meeting Supplement, S314.
———(1997b) A model for the layered upper mantle. Physics of the Earth and Planetary Interiors, 100, 197–212.
Gasparik, T. and Drake, M.J. (1995) Partitioning of elements among two silicate perovskites, superphase B, and volatile-bearing melt at 23 GPa and 1500–1600 °C. Earth and Planetary Science Letters, 134, 307–318.
Gasparik, T. and Litvin, Y.A. (1997) Stability of Na₂Mg₂Si₂O₇ and melting relations on the forsterite-jadeite join at pressures up to 22 GPa. European Journal of Mineralogy, 9, 311–326.
Gasparik, T., Parise, J.B., Eiben, B.A., and Hriljac, J.A. (1995) Stability and structure of a new high-pressure silicate, Na₁.₈Ca₁.₁Si₆O₁₄. American Mineralogist, 80, 1269–1276.
Hilst, R. van der, Engdahl, R., Spakman, W., and Nolet, G. (1991) Tomographic imaging of subducted lithosphere below northwest Pacific island arcs. Nature, 353, 37–43.
Kanzaki, M., Stebbins, J.F., and Xue, X. (1991) Characterization of quenched high-pressure phases in CaSiO₃ system by XRD and ²⁹Si NMR. Geophysical Research Letters, 18, 463–466.
Kelsey, C.H. and McKie, D. (1964) The unit-cell of aenigmatite. Mineralogical Magazine, 33, 986–1001.
Knoche, R., Angel, R.J., Seifert, F., and Fliervoet, T.F. (1998) Complete substitution of Si for Ti in titanite Ca(Ti₁₋ₓSiₓ)ⁿⁱSiⁱᵛO₅. American Mineralogist, 83, 1168–1175.
Kubo, A., Suzuki, T., and Akaogi, M. (1997) High-pressure phase equilibria in the system CaTiO₃-CaSiO₃: stability of perovskite solid solutions. Physics and Chemistry of Minerals, 24, 488–494.
Leinenweber, K., Grzechnik, A., Voorhees, M., Navrotsky, A., Yao, A., and McMillan, P.F. (1997) Structural variation in Ca(TiₓSi₁₋ₓ)O₃ perovskites (1 > x > 0.65) and the ordered phase Ca₂TiSiO₆. Physics and Chemistry of Minerals, 24, 528–534.
Lesher, C.E. and Walker, D. (1988) Cumulate maturation and melt migration in a temperature gradient. Journal of Geophysical Research, 93, 10295–10311.
Liebau, F. (1985) Structural Chemistry of Silicates, 104 p. Springer-Verlag, Berlin.
Litvin, Y.A. and Gasparik, T. (1993) Melting of jadeite to 16.5 GPa and melting relations on the enstatite-jadeite join. Geochimica et Cosmochimica Acta, 57, 2033–2040.
Merlino, S. (1972) X-ray crystallography of krinovite. Zeitschrift für Kristallographie, 136, 81–88.
Pacalo, R.E.G. and Gasparik, T. (1990) Reversals of the orthoenstatite-clinoenstatite transition at high pressures and high temperatures. Journal of Geophysical Research, 95, 15853–15858.
Pacalo, R.E.G. and Parise, J.B. (1992) Crystal structure of superhydrous

B, a hydrous magnesium silicate synthesized at 1400 °C and 20 GPa. American Mineralogist, 77, 681–684.

Ringwood, A.E. (1967) The pyroxene-garnet transformation in the earth's mantle. Earth and Planetary Science Letters, 2, 255–263.

Ringwood, A.E. and Major, A. (1966) Synthesis of Mg_2SiO_4-Fe_2SiO_4 spinel solid solutions. Earth and Planetary Science Letters, 1, 241–245.

———(1971) Synthesis of majorite and other high-pressure garnets and perovskites. Earth and Planetary Science Letters, 12, 411–418.

Woodland, A.B. and Angel, R.J. (1997) Reversal of the orthoferrosilite-high-P clinoferrosilite transition, a phase diagram for $FeSiO_3$ and implications for the mineralogy of the Earth's upper mantle. European Journal of Mineralogy, 9, 245–254.

Young, V.G. Jr. (1997) UNTWIN: A program for creating an HKLF 5 reflection file from the twin law, the metric tensor and an HKLF 4 reflection file. Unpublished computer program.